NeuroImage: Clinical 37 (2023) 103321

Contents lists available at ScienceDirect

NeuroImage: Clinical

journal homepage: www.elsevier.com/locate/ynicl

Longitudinal changes in ^{18}F-Flutemetamol amyloid load in cognitively intact *APOE4* carriers versus noncarriers: Methodological considerations

Emma S. Luckett [a,b], Jolien Schaeverbeke [a,b], Steffi De Meyer [a,b,c], Katarzyna Adamczuk [d], Koen Van Laere [e,f], Patrick Dupont [a,b], Rik Vandenberghe [a,b,g,*]

[a] *Laboratory for Cognitive Neurology, Department of Neurosciences, Leuven Brain Institute, KU Leuven, Leuven, Belgium*
[b] *Alzheimer Research Centre KU Leuven, Leuven Brain Institute, Leuven, Belgium*
[c] *Laboratory for Molecular Neurobiomarker Research, KU Leuven, Leuven, Belgium*
[d] *Clario, Newark, CA, USA*
[e] *Division of Nuclear Medicine, UZ Leuven, Leuven, Belgium*
[f] *Nuclear Medicine and Molecular Imaging, Department of Imaging and Pathology, KU Leuven, Leuven, Belgium*
[g] *Neurology Department, University Hospitals Leuven, Leuven, Belgium*

ARTICLE INFO

Keywords:
Alzheimer's disease
APOE4
Longitudinal study
Amyloid-PET
^{18}F-Flutemetamol
Reference region
Amyloid accumulation

ABSTRACT

Purpose: Measuring longitudinal changes in amyloid load in the asymptomatic stage of Alzheimer's disease is of high relevance for clinical research and progress towards more efficacious, timely treatments. Apolipoprotein E ε4 (*APOE4*) has a well-established effect on the rate of amyloid accumulation. Here we investigated which region of interest and which reference region perform best at detecting the effect of *APOE4* on longitudinal amyloid load in individuals participating in the Flemish Prevent Alzheimer's Disease Cohort KU Leuven (F-PACK).

Methods: Ninety cognitively intact F-PACK participants (baseline age: 68 (52–80) years, 46 males, 42 *APOE4* carriers) received structural MRI and ^{18}F-Flutemetamol PET scans at baseline and follow-up (6.2 (3.4–10.9) year interval). Standardised uptake value ratios (SUVRs) and Centiloids (CLs) were calculated in a composite cortical volume of interest ($SUVR_{comp}$/CL) and in the precuneus ($SUVR_{prec}$), and amyloid rate of change derived: (follow-up amyloid load – baseline amyloid load) / time interval (years). Four reference regions were used to derive amyloid load: whole cerebellum, cerebellar grey matter, eroded subcortical white matter, and pons.

Results: When using whole cerebellum or cerebellar grey matter as reference region, *APOE4* carriers had a significantly higher $SUVR_{comp}$ amyloid rate of change than non-carriers ($p_{corr} = 0.004$, $t = 3.40$ (CI 0.005–0.018); $p_{corr} = 0.036$, $t = 2.66$ (CI 0.003–0.018), respectively). Significance was not observed for eroded subcortical white matter or pons ($p_{corr} = 0.144$, $t = 2.13$ (CI 0.0003–0.008); $p_{corr} = 0.116$, $t = 2.22$ (CI 0.005–0.010), respectively). When using CLs as the amyloid measurement, and whole cerebellum, *APOE4* carriers had a higher amyloid rate of change than non-carriers ($p_{corr} = 0.012$, $t = 3.05$ (CI 0.499–2.359)). Significance was not observed for the other reference regions. No significance was observed with any of the reference regions and amyloid rate of change in the precuneus ($SUVR_{prec}$).

Conclusion: In this cognitively intact cohort, a composite neocortical volume of interest together with whole cerebellum or cerebellar grey matter as reference region are the methods of choice for detecting *APOE4*-dependent differences in amyloid rate of change.

Abbreviations: AAL, Automated Anatomical Labelling atlas; AD, Alzheimer's Disease; AMYPAD, The amyloid imaging to prevent Alzheimer's disease study; APOE4, Apolipoprotein E ε4; BDNF, Brain Derived Neurotrophic Factor; CI, Confidence interval; CDR, Clinical Dementia Rating; CGM, Cerebellar Grey Matter; CL, Centiloids; ESWM, Eroded subcortical white matter; F-PACK, Flemish Prevent AD Cohort KU Leuven; GM, Grey Matter; HC, Healthy control; MMSE, Mini Mental State Examination; MRI, Magnetic Resonance Imaging; PET, Positron Emission Tomography; SUVR, Standardised Uptake Value Ratio; $SUVR_{comp}$, Standardised Uptake Value Ratio in the Composite cortical volume of interest; $SUVR_{prec}$, Standardised Uptake Value Ratio in the precuneus; WCER, Whole cerebellum; WM, White matter.

* Corresponding author at: Neurology Department, University Hospitals, Leuven, Herestraat 49, 3000 Leuven, Belgium.
E-mail address: rik.vandenberghe@uz.kuleuven.ac.be (R. Vandenberghe).

https://doi.org/10.1016/j.nicl.2023.103321
Received 23 June 2022; Received in revised form 12 December 2022; Accepted 4 January 2023
Available online 5 January 2023

1. Introduction

Amyloid positron emission tomography (PET) is widely used to determine the presence of amyloid-β plaques in vivo (Jack et al., 2018), as well as in clinical trial settings to determine those individuals suitable for trial recruitment. Amyloid-PET can be used to establish target engagement, in addition to using amyloid load changes as a potential surrogate marker for evaluating the effect of amyloid-lowering drugs. *APOE4*, the largest genetic risk factor for sporadic Alzheimer's disease (AD) (Corder et al., 1993), increases the susceptibility of amyloid aggregation (Villemagne et al., 2011). *APOE4* is also associated with a higher rate of amyloid deposition (in a gene dose-dependent manner) in the asymptomatic, mild cognitive impairment and AD stages of disease (Grimmer et al., 2010; Villemagne et al., 2011; Yamazaki et al., 2019). Furthermore, *APOE4* is also associated with a higher risk of initiating amyloid deposition (Burnham et al., 2020), as well as a higher rate of change specifically in the precuneus (an early AD-affected region (Insel et al., 2020; Mishra et al., 2018; Palmqvist et al., 2017)), for those aged below 80 years (Vlassenko et al., 2012).

Most studies evaluated changes in individuals with impaired cognition, or combined healthy controls with patients. However, amyloid pathology can appear more than a decade prior to symptom onset, considered to be the asymptomatic stage of AD (Villemagne et al., 2013). Therefore, there is a requirement for independent studies investigating the most sensitive method for studying amyloid accumulation in this early stage of AD.

^{18}F-Flutemetamol is a radiotracer that has a high affinity for brain amyloid plaques, can discriminate AD cases from controls, and shows high concordance with histopathological neuritic amyloid plaque density (Reinartz et al., 2022; Salloway et al., 2017). Despite relative concordance of amyloid-PET acquisition and processing, the choice of reference region differs largely between sites, in particular when working cross-sectionally versus longitudinally. A reference region needs to be defined that is preferably devoid of amyloid plaques over time, but also can be used to detect meaningful and biologically relevant changes in the brain, whilst reducing noise. Previous studies have shown that cerebellar grey matter (CGM) and pons fulfil the requirements for a suitable reference region, and have as such been used in many cross-sectional and longitudinal studies, especially CGM. However, more recent studies (using ^{18}F-Florbetapir) have implicated eroded subcortical white matter (ESWM) as being superior for longitudinal studies (Blautzik et al., 2017; Chen et al., 2015; Chiao et al., 2019; Landau et al., 2015).

Further to this, the Centiloid (CL) scale has been developed, allowing for the standardisation of amyloid measurements across various amyloid radiotracers on a common (CL) scale (Klunk et al., 2015), utilising the whole cerebellum (WCER) as a reference region. In recent years, CLs have become an increasingly common way to express amyloid load that can be applied and compared across amyloid-PET tracers. This allows for the pooling of data across centres, as well as data processed with different methods of acquisition and pre-processing.

It is now firmly established that there is an association between *APOE4* and the clinical development of AD, as well as the accumulation of amyloid plaques in the brain over time in the asymptomatic phase (Villain et al., 2012). Since there is no clear consensus on which reference region is optimal for semi-quantification of amyloid rate of change, in the present study we investigated the effect of four reference regions on longitudinal amyloid load (WCER, CGM, ESWM and pons) in cognitively intact elderly individuals. Since *APOE4* enhances amyloid accumulation over time (Lim and Mormino, 2017; Mishra et al., 2018; Villemagne et al., 2011), we aimed to investigate which reference region most sensitively quantifies this effect both in a composite region of interest and the precuneus, in exclusively cognitively intact individuals, some of whom are in the asymptomatic phase of AD.

2. Material and methods

2.1. Study participants

The Laboratory for Cognitive Neurology follows a deeply phenotyped cohort of 180 community-recruited healthy older adults, known as the Flemish Prevent AD Cohort KU Leuven (F-PACK), who were recruited in three waves of 60 participants from 2009 to 2015 (waves one to three). Inclusion criteria included being aged between 50 and 80 years old, Mini Mental State Examination (MMSE) score $\geq$ 27, Clinical Dementia Rating (CDR) score = 0, and neuropsychological test scores within published norms (Adamczuk et al., 2013; Schaeverbeke et al., 2021). Recruitment was stratified based on *APOE* status (ε*4* present or absent) and Brain Derived Neurotrophic Factor (*BDNF*) status (66 *met* present or absent), such that per five-year age bin there was an equal number of individuals in each factorial cell, matched for age, sex and education.

A subset of 90 participants consented to follow-up scanning, and have thus received a follow-up ^{18}F-Flutemetamol PET scan, T1-weighted structural MRI and blood sampling, with a median time interval of 6.2 (3.4–10.9) years after baseline. All participants were cognitively intact at the time of the follow-up PET scan and are being followed over a 10-year period, with two-yearly neuropsychological evaluations. Written informed consent was obtained from all participants in accordance with the Declaration of Helsinki. The protocol was approved by the Ethics Committee University Hospitals Leuven.

2.2. Imaging

2.2.1. Structural MRI

A high resolution T1-weighted structural MRI was acquired at baseline and follow-up for the PET processing procedure described in Section 2.2.3. Scans were performed using a 3 T Philips Achieva dstream 32-channel headcoil MRI scanner (Philips, Best, The Netherlands). All baseline scans and 65 follow-up scans were acquired using a 3D turbo field echo sequence: inversion time = 900 ms; repetition time = 9.6 ms; echo time = 4.6 ms; flip angle = 8°; field of view = 250 × 250 mm; 182 slices; voxel size 0.98 × 0.98 × 1.2 mm^3. Twenty-two follow-up scans were acquired using a 3D magnetisation-prepared rapid gradient-echo sequence as they were acquired as part of the Amyloid imaging to prevent Alzheimer's disease study (AMYPAD): repetition time = 6.6 ms; echo time = 3.1 ms; flip angle = 9°; field of view = 270 × 252 mm; 170 slices; voxel size 1.05 × 1.05 × 1.2 mm^3. Three individuals refused a follow-up MRI scan.

2.2.2. ^{18}F-Flutemetamol PET

^{18}F-Flutemetamol PET scans were acquired on a 16-slice Biograph PET/CT scanner (Siemens, Erlangen, Germany), at baseline and follow-up for all 90 participants, with a net injected intravenous dose of 149 MBq (127–163 MBq) and 167 MBq (77–198 MBq), respectively, and acquisition window of 90–120 min post-injection. Four participants were scanned 90–110 min post injection due to scan acquisition prior to a protocol amendment. Data were reconstructed as frames of five minutes using ordered subsets expectation maximisation and smoothed with a 5 mm full width at half maximum 3D Gaussian filter, as part of the reconstruction, given the spatial resolution of the scanner is 4.6 mm full width at half maximum 1 cm off centre measured with the NEMA protocol. All baseline and 72 follow-up scans were reconstructed with five iterations in eight subsets. Eighteen follow-up scans were reconstructed as four iterations in 21 subsets, as they were acquired with the AMYPAD protocol. Image processing of the reconstructed PET data was performed using in-house developed scripts using Statistical Parametric Mapping version 12 (SPM12, Wellcome Trust Centre for Neuroimaging, London, UK, https://www.fil.ion.ucl.ac.uk/spm) running on MATLAB R2018b (Mathworks, Natick, MA, USA), as previously described (Adamczuk et al., 2016, 2013; Koole et al., 2009; Schaeverbeke et al., 2022;

Vandenberghe et al., 2010). Briefly, frames were realigned to the first frame and summed to a single sumPET. The MRI was used for coregistration and normalisation of the sumPET to Montreal Neurological Institute space using a segmentation approach. We did not use partial volume correction (Minhas et al., 2018; Schwarz et al., 2019).

2.2.3. Image analysis

The (mean) standardised uptake value ratios (SUVRs) from the spatially normalised images (voxel size: $2 \times 2 \times 2$ mm^3) were calculated in a composite cortical VOI ($SUVR_{comp}$), derived from the Automated Anatomic Labelling atlas (AAL) (Tzourio-Mazoyer et al., 2002). This composite VOI included the following bilateral regions: frontal (AAL areas 3–10, 13–16, 23–28), parietal (AAL 57–70), anterior cingulate (AAL 31–32), posterior cingulate (AAL 35–36) and lateral temporal (AAL 81–82, 85–90) (Adamczuk et al., 2013). The composite VOI was masked with the participant-specific grey matter (GM) segmentation map (intensity threshold of GM voxels > 0.3, (Adamczuk et al., 2013).

Our secondary PET outcome measure was calculating SUVRs specifically in a precuneus volume of interest ($SUVR_{prec}$, AAL 67–68) as this region is known to be affected by amyloid deposition early in the disease progression, thus allowing us to determine early amyloid changes (Palmqvist et al., 2017). The precuneus VOI was masked by the subject-specific GM map (GM intensity threshold > 0.3).

SUVRs were calculated using four reference regions of interest: whole cerebellum (WCER), cerebellar grey matter (CGM), eroded subcortical white matter (ESWM) and pons. The WCER VOI was defined as AAL areas 91–116 and included both white and grey matter. The CGM VOI was defined as AAL areas 91–108 and was masked by the participant-specific GM map (GM intensity threshold > 0.3) (Adamczuk et al., 2013). The ESWM VOI was derived from the participant-specific whole-brain WM map from the MRI segmentation procedure for the PET processing. An in-house script eroded the WM map with an erosion kernel of $3 \times 3 \times 3$ voxels, and a WM voxel inclusion intensity threshold > 0.5 (to ensure that despite the erosion, inclusion of GM voxels was minimised given proximity to the neighbouring GM cortical regions). The original pons VOI was manually drawn on the SPM12 T1 template (13 axial slices of 2 mm, drawing from $x = 0$, $y = -12$, $z = -32$ (Adamczuk et al., 2016). This VOI was then masked by the participant-specific WM map (WM intensity threshold > 0.3). Fig. 1 shows an example of each of the reference regions used.

Amyloid rate of change was derived for $SUVR_{comp}$ and $SUVR_{prec}$, which was defined as: [follow-up amyloid – baseline amyloid]/time interval (years).

2.2.4. Conversion of SUVRs to Centiloids

As a further analysis, we examined whether the findings obtained in the primary analysis, were also applicable when CLs, rather than $SUVR_{comp}$, were used as the parameter for amyloid measurement using a different approach that is standardised. To allow for $SUVR_{comp}$ from each reference region to be on the CL scale, CL conversion formulas were generated (Klunk et al., 2015). First the PET images were reprocessed with an acquisition window 90–110 min post injection as this is what the standard CL method uses. The level-1 analysis was replicated in a previous study from our Laboratory, which allowed the anchor points to be established (de Meyer et al., 2020). The level-2 analysis was already performed in this previous study to generate a CL conversion formula when using CGM as a reference region, which is defined as $127.6 \times SUVR - 149$ (de Meyer et al., 2020). For determining conversion formulas for the other reference regions see Supplementary Information.

The following CL conversion formulas for each of the reference regions were obtained: $CL_{\text{whole cerebellum}} = 140 \times SUVR - 160$, $CL_{\text{eroded subcortical white matter}} = 280 \times SUVR - 140$, $CL_{\text{pons}} = 230 \times SUVR - 120$. The CL conversion formulas were then used to convert the $SUVR_{comp}$ for each reference region from the F-PACK cohort to CLs for use in further analyses. Amyloid rate of change for CLs was also calculated as above.

2.2.5. Determination of amyloid positivity

To determine amyloid-positive from amyloid-negative participants when using SUVRs, we calculated thresholds for each reference region for the composite VOI, using an independent dataset consisting of AD

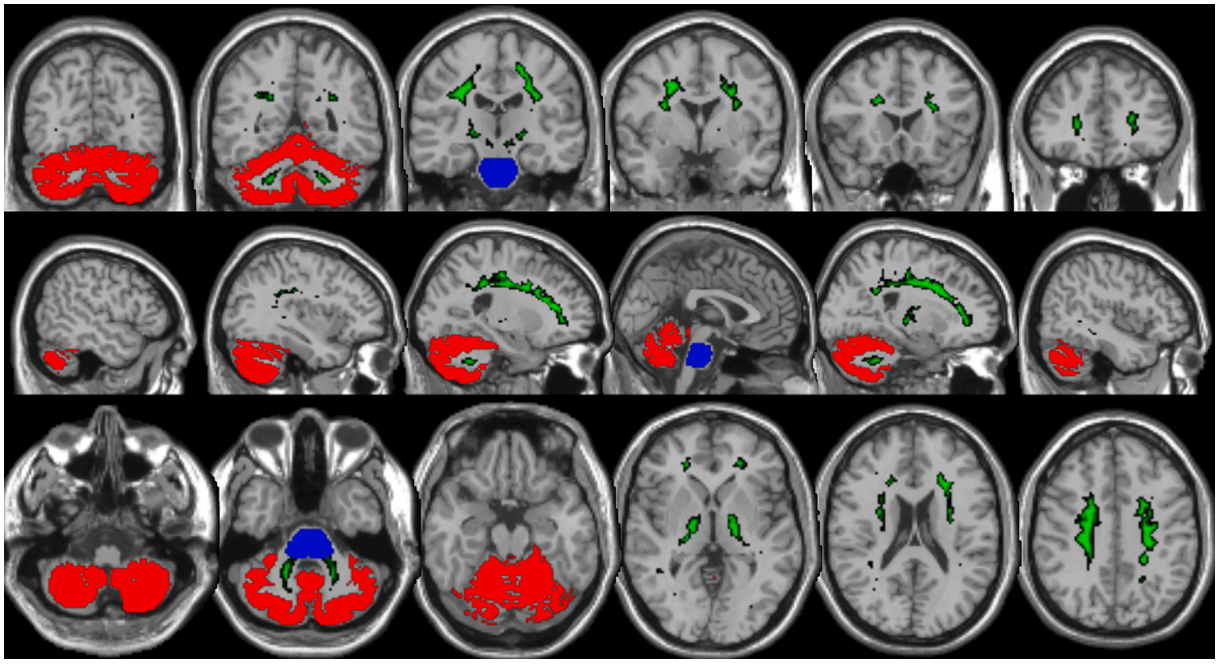

Fig. 1. Example reference regions used to calculate amyloid load. Cerebellar grey matter (red), eroded subcortical white matter (green), and pons (blue) reference regions overlaid on the SPM standard T1 MRI template. Whole cerebellum not shown to highlight the cerebellar grey matter reference region used. All reference regions are subject-specific, based on the participant's own grey matter/white matter MRI segmentations. Therefore, the highlighted regions depicted do not represent the exact reference regions used when calculating amyloid load for each participant. Numbers refer to the *x*-, *y*-, and *z*- positions in MNI space of the coronal, sagittal and transverse slices. (For interpretation of the references to colour in this figure legend, the reader is referred to the web version of this article.)

patients (N = 25, 71 (56–81) years old, 12 males, 15 (8–24) years of education, MMSE = 23 (19–26), CDR = 1 (0.5–1)) and elderly healthy controls (HC, N = 14, aged 71 (56–78) years, 8 males, 13 (8–18) years of education, MMSE 28.5 (27–30), CDR = 0)) (Vandenberghe et al., 2010). We used the PET processing method detailed in Section 2.2.3 to generate $SUVR_{comp}$ for each individual, for each reference region, and then used the mean $SUVR_{comp}$ to generate the thresholds for amyloid positivity using the method described previously (Adamczuk et al., 2013; Vandenberghe et al., 2010). This procedure bases the threshold on the statistical difference between the AD and HC groups using the following:

$$factor = \frac{Mean\ SUVR_{comp}AD - Mean\ SUVR_{comp}HC}{SD\ SUVR_{comp}AD + SD\ SUVR_{comp}HC}$$

$$SUVR_{comp}threshold = Mean\ SUVR_{comp}AD - factor \times SD\ SUVR_{comp}AD$$

The CGM threshold for $SUVR_{comp}$ had previously been calculated in our Laboratory and corresponded to 1.38 (Adamczuk et al., 2013). The $SUVR_{comp}$ threshold for WCER = 1.55, ESWM = 0.68, and pons = 0.84.

The same procedure was then performed for the precuneus VOI, to generate thresholds for positivity for this specific region for visualisation purposes. These corresponded to: WCER = 1.53, CGM = 1.85, ESWM = 0.70, and pons = 0.83.

To have a standardised approach, the CL threshold for amyloid positivity corresponded to = 23.5, a widely accepted pathologically validated threshold (la Joie et al., 2019).

2.3. Statistical analyses

Statistical analyses and figures were performed and made in R, version 4.1.3 (2022–03-10; The R Foundation for Statistical Computing; https://cran.r-project.org/). Prior to analyses Shapiro-Wilk tests were used to determine data normality.

Depending on data normality, cohort characteristics were assessed between *APOE4* carriers and non-carriers using Wilcoxon rank sum tests with continuity correction or Welch two-sample *t*-tests for continuous data, and χ^2 tests for categorical data. *p*-values were considered significant when meeting a two-tailed threshold of $\alpha < 0.05$.

Despite thorough quality control of image acquisition and processing, there is one participant who had a disproportionate decrease in amyloid load between baseline and follow-up when amyloid load calculated with ESWM. There was no explanation found for this so primary and secondary analyses were repeated after the removal of these values.

2.3.1. Primary analyses

Linear mixed effects models were performed using the R package *nlme* with the *restricted maximum likelihood estimation* and *optimMethod* = *"SANN"* using SUVR as dependent variable, with the interaction of *APOE4* status and time interval as fixed effects, correcting for age, sex and education. Participant ID and time interval were used as random effects. This allowed us to determine whether *APOE4* carriers had an increase in amyloid over time interval compared to non-carriers. Amyloid change in *APOE4* carriers compared to non-carriers per year from the LME model is reported, with 95 % confidence intervals (CIs) and the corresponding model *t*- and *p*-values of the interaction.

Identical analyses were then performed using $SUVR_{prec}$ values from each reference region to determine differences in amyloid change in the precuneus.

Furthermore, we evaluated amyloid change when using CLs. Thus, the above analyses using $SUVR_{comp}$ were also performed using CLs for each reference region.

Inference was based on an uncorrected $p < 0.05$ threshold divided by the number of reference regions (N = 4).

2.3.2. Secondary analyses

A Friedman's repeated measures was performed to determine whether there were significant differences between the $SUVR_{comp}$ rate of change values from each reference region across all participants. Kendall's *W* effect size was calculated, and if the Friedman's repeated measures was significant, multiple pairwise-comparisons were performed using paired Wilcoxon matched pairs signed rank tests with Bonferroni correction. This was also performed for the composite VOI with CLs as amyloid measurement.

Linear regression analyses were performed using each amyloid measurement to determine whether there was an association between baseline amyloid load and amyloid rate of change with each reference region (baseline age, sex and *APOE4* status as covariates).

3. Results

The cohort characteristics for the participants included in the present study can be found in Table 1, stratified for *APOE4* status. Only education was significantly different between the two groups, where *APOE4* carriers had a significantly higher number of years of education (p = 0.049). At the neuropsychological follow-up closest to the follow-up amyloid-PET scan, two participants had a CDR of 0.5, with corresponding MMSEs of 26 (*APOE* ε3ε3) and 28 (*APOE* ε3ε4) out of 30.

When determining amyloid positivity using $SUVR_{comp}$, the number of amyloid positive individuals increased at follow-up with all reference regions (Table 2, Fig. 2a-d). Fig. 2e-h shows the amyloid change in the precuneus. When determining amyloid positivity using CLs, the number of amyloid positive individuals also increased at follow-up for all reference regions (Table 2, Fig. 2i-l).

3.1. Primary analyses

For $SUVR_{comp}$, *APOE4* carriers had a significant increase in amyloid per year than non-carriers when using WCER or CGM as reference region, with high corresponding *t*-values (Table 3, Fig. 2a and b). No significant differences between groups were observed for ESWM or pons (Table 3, Fig. 2c and d). When the outlier was removed, the significance remained for WCER, but was lost for CGM (p = 0.015).

There were no significant differences in amyloid change between *APOE4* groups when using $SUVR_{prec}$ for any of the reference regions (Table 3, Fig. 2e-h). When the outlier was removed there was still no significance observed.

When using CLs and the composite cortical VOI, *APOE4* carriers had a significantly higher amyloid rate of change than non-carriers when WCER was used as a reference region (Table 3, Fig. 2i). Significance was not observed for the other reference regions (Table 3, Fig. 2j-l). When the outlier was removed the significance from the main analyses remained.

None of the other fixed effects were significant in any of the models.

3.2. Secondary analyses

The Friedman's repeated measures highlighted a significant difference in $SUVR_{comp}$ amyloid rate of change between the different reference regions (χ^2 = 21.9, $p = 6.78 \times 10^{-5}$). However, the effect size was small (W = 0.08). Multiple pairwise-comparisons showed that $SUVR_{comp}$ rate of change was lower when using ESWM as a reference region compared to when WCER, CGM or pons were used as reference regions (Table 4, Fig. 3a). When the outlier was removed, the overall significance remained (χ^2 = 21.1, $p = 9.81 \times 10^{-5}$, W = 0.08), as did the significance for the multiple pairwise-comparisons (Table 4).

When using CLs as the amyloid measurement, the Friedman's repeated measures highlighted a significant difference in amyloid rate of change between the different reference regions (χ^2 = 45.3, $p = 7.81 \times 10^{-10}$). However, the effect size was small (W = 0.17). Multiple pairwise-comparisons highlighted significant differences between the CL-based rate of change values of WCER and CGM (CGM lower group median), WCER and ESWM (ESWM lower group median), WCER and pons (WCER

Table 1
Baseline characteristics stratified for *APOE4* status for F-PACK participants.

	APOE4 non-carriers	*APOE4* carriers	Statistics
Sex (Male/Female)	23/25	23/19	$\chi^2 = 0.19$, $p = 0.66$
BDNF codon 66 *met* carriers	24	23	$\chi^2 = 0.06$, $p = 0.81$
Age (years)	67 (52–80)	68 (56–79)	$T = -0.10$, $p = 0.92$
Education (years)	14 (8–20)	16 (9–24)	**$T = 2.00$, $p = 0.049$**
MMSE (/30)	29 (27–30)	29 (27–30)	$W = 1012$, $p = 0.98$
CDR	0	0	NA
AVLT TL (/75)	48 (30–69)	46 (35–68)	$T = -0.25$, $p = 0.80$
AVLT %DR	86 (30–108)	86 (58–108)	$W = 1020$, $p = 0.93$
Mean BSRT TR (/12)	8 (6–11)	8 (5–11)	$W = 888.5$, $p = 0.32$
BSRT DR (/12)	8 (2–12)	8 (3–12)	$W = 947$, $p = 0.62$
BNT (/60)	57 (46–60)	57 (41–60)	$W = 1030$, $p = 0.86$
AVF (# words/1 min)	23 (14–40)	24 (14–42)	$T = 0.80$, $p = 0.43$
LVF (# words)	36 (14–65)	38 (9–64)	$T = 0.21$, $p = 0.84$
PALPA49 (/30)	28 (20–30)	27 (23–30)	$W = 987$, $p = 0.87$
RPM (/60)	46 (22–57)	45 (22–57)	$W = 896$, $p = 0.37$
TMT B/A	2 (1–5)	2 (1–5)	$T = 0.58$, $p = 0.57$
Baseline $SUVR_{comp}$ WCER	1.199 (1.047–1.360)	1.227 (1.034–1.922)	$W = 551.5$, $p = 0.32$
Baseline $SUVR_{comp}$ CGM	1.218 (1.092–1.372)	1.242 (1.062–2.072)	$W = 561$, $p = 0.26$
Baseline $SUVR_{comp}$ ESWM	0.484 (0.404–0.589)	0.498 (0.445–0.755)	$W = 611$, $p = 0.07$
Baseline $SUVR_{comp}$ Pons	0.664 (0.585–0.728)	0.677 (0.620–0.948)	$W = 582$, $p = 0.15$
Time interval between amyloid-PET (years)	6 (4–11)	6 (3–10)	$W = 812$, $p = 0.11$

Data are reported as median and range (minimum to maximum) for continuous variables, and numerical for categorical variables. Statistical tests used for continuous data are Wilcoxon rank sum test with continuity correction, or Welch two sample *t*-test, depending on the normality of the data. Chi-squared tests have been used for categorical data. N = 90. Significant results are in bold. Abbreviations: AVF = Animal Verbal Fluency Test; AVLT DR/TL = Rey Auditory Verbal Learning Test Delayed Recall/Total Learning; BNT = Boston Naming Test; BSRT DR/TR = Buschke Selective Reminding Test Delayed Recall/Total Retention; CDR = Clinical Dementia Rating scale; CGM = Cerebellar grey matter; ESWM = Eroded subcortical white matter; LVF = Letter Verbal Fluency Test; MMSE = Mini Mental State Examination; PALPA49 = Psycholinguistic Assessment of Language Processing in Aphasia (PALPA) subtest 49; RPM = Raven's Progressive Matrices; $SUVR_{comp}$ = Standardised uptake value ratio in the composite region; TMT B/A = Trail Making Test part B divided by part A; WCER = Whole cerebellum.

lower group median), CGM and pons (CGM lower group median), and ESWM and pons (ESWM lower group median, Table 4, Fig. 3b). When the outlier was removed, the overall significance remained ($\chi^2 = 45.5$, $p = 7.17^{-10}$, $W = 0.17$), and multiple pairwise-comparisons highlighted the same significant differences as above.

When using $SUVR_{comp}$, higher baseline amyloid load was significantly associated with increased amyloid rate of change for WCER, CGM, and pons as reference regions, but not ESWM as reference region (Table 5, Fig. 4a-d). When the outlier was removed, significance remained for all reference regions from the main analyses, and was also present for ESWM (Table 5).

There was a significant association between higher baseline precuneus amyloid load and increased composite amyloid rate of change for all reference regions (Table 5, Fig. 4e-h). When the outlier was removed, significance remained for all reference regions.

As with $SUVR_{comp}$, when using CLs, higher baseline amyloid load was significantly associated with increased amyloid rate of change for WCER, CGM, and pons as reference regions, but not ESWM as reference region (Table 5, Fig. 4i-l). When the outlier was removed, significance remained for all reference regions from the main analyses, and was also present for ESWM (Table 5).

Table 2
Number of amyloid positive individuals based on thresholds for positivity.

	Reference region	Amyloid positive (N (%))	
		Baseline	Follow-up
$SUVR_{comp}$	WCER	4 (4 %)	8 (9 %)
	CGM	9 (10 %)	19 (21 %)
	ESWM	5 (6 %)	10 (11 %)
	Pons	3 (3 %)	7 (8 %)
Centiloids	WCER	16 (18 %)	25 (28 %)
	CGM	11 (12 %)	19 (21 %)
	ESWM	12 (14 %)	19 (21 %)
	Pons	15 (17 %)	32 (36 %)

Thresholds for positivity for whole cerebellum = 1.55, cerebellar grey matter = 1.38, eroded subcortical white matter = 0.68, and pons = 0.84. Threshold for amyloid positivity when using Centiloids = 23.5 (la Joie et al., 2019). Significant results are in bold. N = 90. Subjects positive at baseline and negative at follow-up for each reference region were as follows: $SUVR_{comp}$ WCER and Pons = 0; $SUVR_{comp}$ CGM and ESWM = 1; CL WCER, ESWM, Pons = 2; CL GCM = 1. $SUVR_{comp}$ acquisition window = 90–120 min post injection; CL acquisition window = 90–110 min post injection. Abbreviations: CGM = Cerebellar grey matter; ESWM = Eroded subcortical white matter; $SUVR_{comp}$ = Standardised uptake value ratio in the composite region; WCER = Whole cerebellum.

4. Discussion

Our study showed that when using WCER or CGM as reference region, $SUVR_{comp}$ amyloid rate of change in a composite region of interest highlighted the early differential effect of *APOE4*, in contrast to ESWM. This was confirmed when using CLs.

A higher amyloid load, as well as higher rate of amyloid accumulation, has been shown in healthy controls who carry *APOE4*, as well as those (carriers) with MCI and AD (e.g. (Drzezga et al., 2009; Fleisher et al., 2013; Hong et al., 2022; Lehmann et al., 2014; Morris et al., 2010; Reiman et al., 2009; Rowe et al., 2010; Toledo et al., 2019) where the presence of amyloid is detected in *APOE4* carriers at a much earlier age than non-carriers (Fleisher et al., 2013). In the present study, when WCER and CGM were used as reference region, *APOE4* carriers had a significant increase in amyloid per year than non-carriers when using $SUVR_{comp}$, where this was replicated for CLs when WCER used as a reference region. The analyses suggest that *APOE4* carriers have a steeper increase in accumulation with these reference regions, signifying that these reference regions can determine the differential effects of *APOE4* on early amyloid accumulation in the asymptomatic stage of AD.

This may be important when recruiting participants for clinical trials, for example to stratify and recruit at-risk individuals, given we know *APOE4* is the largest genetic risk factor for sporadic AD (Corder et al., 1993). However, it is important to note that *APOE4* carriage is not necessary to develop AD. Thus it is important to realise that those individuals who develop AD without *APOE4*, as well as those at-risk individuals or those in the asymptomatic phase without *APOE4*, may have a different amyloid accumulation profile or trajectory to those that do carry the risk allele. This may mean a different reference region may be more suitable at detecting (early) amyloid accumulation in these individuals. However, given that we are aiming to find differences in an asymptomatic AD population in order to enhance the knowledge about PET processing in these individuals, potentially for recruitment

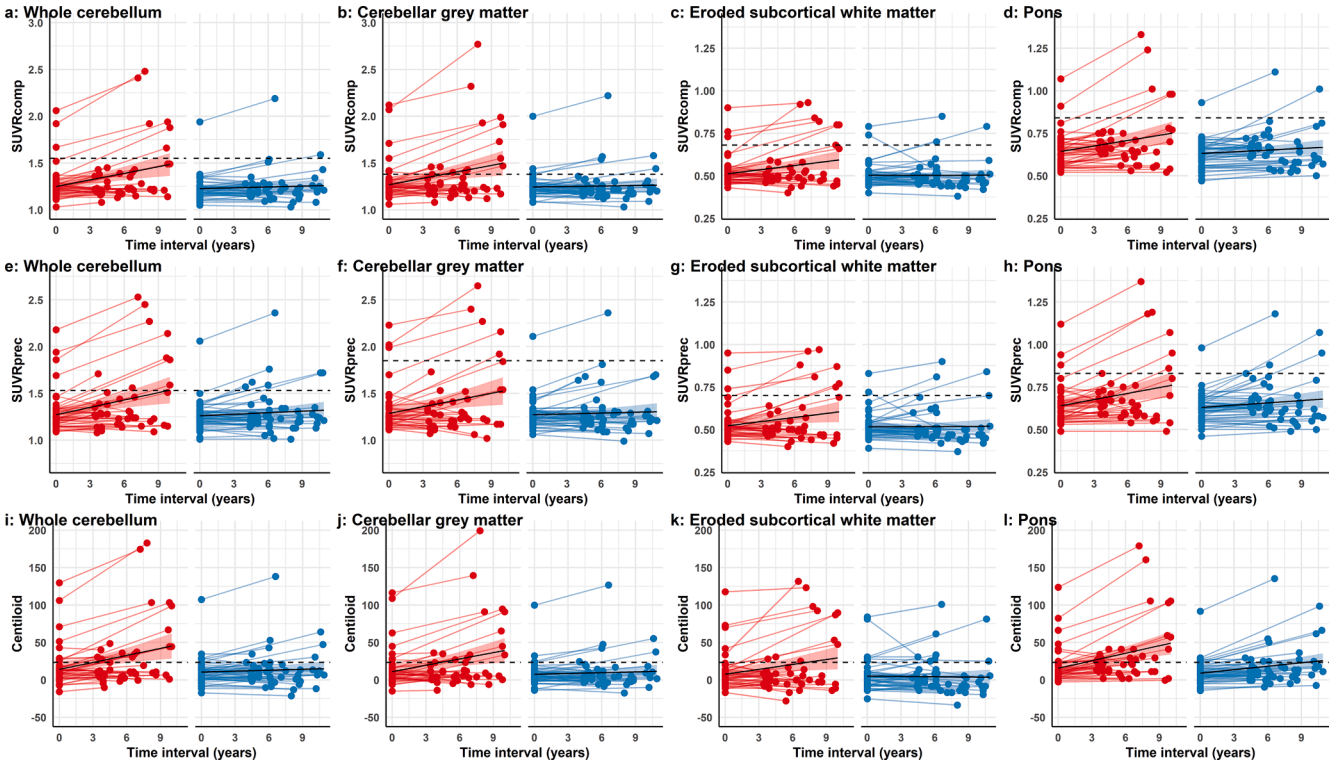

Fig. 2. Change in amyloid for each reference region stratified for *APOE4* polymorphism status (red present, blue absent). $SUVR_{comp}$: (**a**) Whole cerebellum, (**b**) Cerebellar grey matter, (**c**) Eroded subcortical white matter, (**d**) Pons. $SUVR_{prec}$: (**e**) Whole cerebellum, (**f**) Cerebellar grey matter, (**g**) Eroded subcortical white matter, (**h**) Pons. CLs: (**i**) Whole cerebellum, (**j**) Cerebellar grey matter, (**k**) Eroded subcortical white matter, (**l**) Pons. The dotted lines represent the threshold for amyloid positivity. For $SUVR_{comp}$ this is specific for each reference region (WCER =1.55, CGM = 1.38; ESWM = 0.68; pons = 0.84); CL threshold = 23.5 (la Joie et al., 2019). Regression lines are shown with their corresponding standard error. Note the differing scales due to the nature of the values for each reference region. *APOE4* carriers = red ($\varepsilon2\varepsilon4$ N = 2; $\varepsilon3\varepsilon4$ N = 38; $\varepsilon4\varepsilon4$ = 2), *APOE4* non-carriers = blue ($\varepsilon2\varepsilon3$ N = 7; $\varepsilon3\varepsilon3$ N = 41). N = 90. Abbreviations: GCM = cerebellar grey matter; ESWM = eroded subcortical white matter; WCER = whole cerebellum. (For interpretation of the references to colour in this figure legend, the reader is referred to the web version of this article.)

Table 3
Difference in amyloid load at follow-up compared to baseline for each of the amyloid measurements relative to *APOE4* non-carriers using linear mixed effects models.

Amyloid measurement	Reference region	Amyloid rate of change	95 % confidence interval	*t*-value	Interaction *p*-value
$SUVR_{comp}$	WCER	0.011	0.005, 0.018	3.40	**0.001**
	CGM	0.010	0.003, 0.018	2.66	**0.009**
	ESWM	0.004	0.0003, 0.008	2.13	0.036
	Pons	0.005	0.0005, 0.010	2.22	0.029
$SUVR_{prec}$	WCER	0.009	0.001, 0.018	2.22	0.029
	CGM	0.008	−0.0008, 0.017	1.81	0.074
	ESWM	0.003	−0.0009, 0.008	1.57	0.120
	Pons	0.004	−0.001, 0.009	1.59	0.115
Centiloids	WCER	1.429	0.499, 2.359	3.05	**0.003**
	CGM	1.171	0.251, 2.092	2.53	0.013
	ESWM	1.089	−0.092, 2.271	1.83	0.070
	Pons	1.130	0.162, 2.099	2.32	0.023

Amyloid rate of change is the unit of increase in amyloid of *APOE4* carriers compared to non-carriers from the linear mixed effects models. N = 90. Significant results are in bold ($p < 0.013$). SUVR acquisition window = 90–120 min post injection; CL acquisition window = 90–110 min post injection. Abbreviations: CGM = Cerebellar grey matter; ESWM = Eroded subcortical white matter; $SUVR_{comp}$ = Standardised uptake value ratio in the composite region; $SUVR_{prec}$ = Standardised uptake value ratio in the precuneus; WCER = Whole cerebellum.

Table 4
Pairwise comparisons between the rate of change values from each reference region following a significant Friedman's repeated measures, using paired Wilcoxon matched pairs signed rank tests with Bonferroni correction.

Composite amyloid measurement	Reference region comparison (group median)	Adjusted *p*-value
$SUVR_{comp}$	WCER (0.002) versus ESWM (0.00)	$\mathbf{p = 8.52x10^{-4}}$
	CGM (0.001) versus ESWM (0.00)	$\mathbf{p = 0.02}$
	ESWM (0.00) versus pons (0.003)	$\mathbf{p = 5.06x10^{-6}}$
Centiloids	WCER (0.279) versus CGM (0.263)	$\mathbf{p = 0.02}$
	WCER (0.279) versus ESWM (0)	$\mathbf{p = 0.02}$
	WCER (0.279) versus pons (1.06)	$\mathbf{p = 0.0004}$
	CGM (0.263) versus pons (1.06)	$\mathbf{p = 4.6x10^{-5}}$
	ESWM (0) versus pons (1.06)	$\mathbf{p = 1.4x10^{-9}}$

N = 90. SUVR acquisition window = 90–120 min post injection; CL acquisition window = 90–110 min post injection. Significant results are in bold. Abbreviations: CGM = cerebellar grey matter; ESWM = eroded subcortical white matter; $SUVR_{comp}$ = Standardised uptake value ratio in the composite region; WCER = whole cerebellum.

stratification or target engagement, the differences we observe remain valid, especially since *APOE4* is the largest genetic risk factor for AD, increasing risk 3–15-fold with a minor allele frequency of 14 %.

When observing amyloid changes (Fig. 2) one can appreciate the amyloid continuum is represented. However, the CL threshold for positivity detects a higher number of individuals that are amyloid positive compared to the $SUVR_{comp}$ thresholds. This may be due to the different methods of threshold calculation and cohorts used for this, as well as the differing tracers: ^{11}C-PiB for the calculation of the CL threshold, as per the CL tracer and protocol (Klunk et al., 2015)), versus ^{18}F-

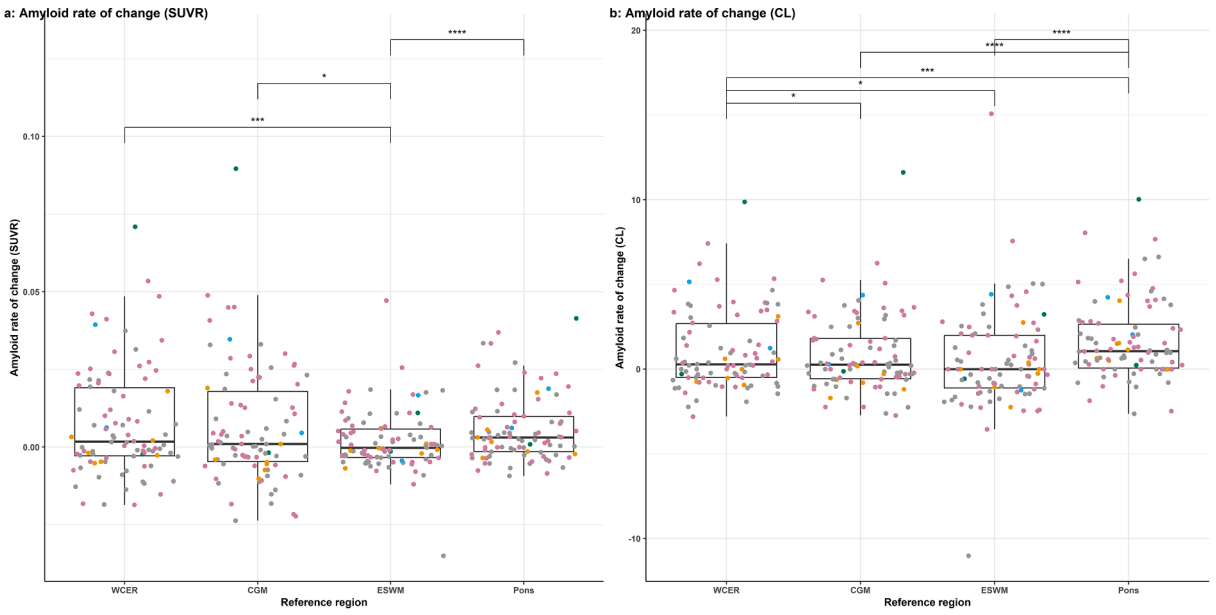

Fig. 3. Amyloid rate of change in the composite VOI differs between the four reference regions. (**a**) $SUVR_{comp}$, (**b**) CL. Data points are coloured by *APOE4* genotype (orange $\varepsilon2\varepsilon3$ N = 7; green $\varepsilon2\varepsilon4$ N = 2; grey $\varepsilon3\varepsilon3$ N = 41; pink $\varepsilon3\varepsilon4$ N = 38; blue $\varepsilon4\varepsilon4$ = 2). N = 90. Significant pairwise comparisons are depicted. Abbreviations: GCM = cerebellar grey matter; ESWM = eroded subcortical white matter; $SUVR_{comp}$ = Standardised uptake value ratio in the composite region; WCER = whole cerebellum. (For interpretation of the references to colour in this figure legend, the reader is referred to the web version of this article.)

Table 5
Regression results with baseline amyloid load as predictor and composite amyloid rate of change as outcome variable, for each reference region and amyloid measurement.

Baseline amyloid	Reference region	Adjusted R^2	β (95 % C.I.)	Baseline amyloid load *p*-value
$SUVR_{comp}$	WCER	0.33	0.05 (0.03–0.07)	**$2.73x10^{-7}$**
	CGM	0.26	0.05 (0.03–0.07)	**$2.22x10^{-6}$**
	Pons	0.16	0.04 (0.02–0.06)	**0.0005**
	ESWM (without outlier)	0.12	0.04 (0.01–0.06)	**0.002**
$SUVR_{prec}$	WCER	0.39	0.05 (0.03–0.06)	**$3.18x10^{-9}$**
	CGM	0.30	0.05 (0.03–0.06)	**$2.49x10^{-7}$**
	ESWM	0.07	0.03 (0.004–0.05)	**0.02**
	Pons	0.22	0.05 (0.03–0.06)	**$1.33x10^{-5}$**
Centiloids	WCER	0.26	0.04 (0.03–0.06)	**$6.21x10^{-6}$**
	CGM	0.26	0.05 (0.03–0.07)	**$1.71x10^{-6}$**
	Pons	0.31	0.06 (0.04–0.08)	**$6.99x10^{-8}$**
	ESWM (without outlier)	0.05	0.03 (0.007–0.06)	**0.01**

Baseline age, sex and *APOE* status are included as covariates. N = 90. Significant results are in bold. SUVR acquisition window = 90–120 min post injection; CL acquisition window = 90–110 min post injection. Abbreviations: CGM = cerebellar grey matter; ESWM = eroded subcortical white matter; $SUVR_{comp}$ = Standardised uptake value ratio in the composite region; $SUVR_{prec}$ = Standardised uptake value ratio in the precuneus; WCER = whole cerebellum.

Flutemetamol for the SUVR thresholds, as was previously described in (Vandenberghe et al., 2010). The acquisition window used in the present study for the SUVR analysis (full window of 90–120 min) was different than in the CL analysis (shortened window of 90–110 min, given this is the method for the CL protocol). Furthermore, to avoid any variability in the definition of amyloid positivity when converting SUVRs to CLs, we chose to use 23.5 given this is an independent and pathologically-defined threshold using WCER as a reference region and ^{11}C-PiB as per the CL protocol allowing for a standardised approach (la Joie et al., 2019). The method used to derive the SUVR thresholds in the present study was not using post mortem data as this was not available to us at the time of analysis and writing, but instead using an independent dataset consisting of AD cases and controls. Nonetheless, the results overall suggest that ESWM is unable to highlight the differential effect of *APOE4* on amyloid rate of change when using SUVRs nor CLs.

It should be noted that the results from the present study do not confirm the suitability of a WM reference region in asymptomatic AD. There are several reasons that may account for this. Firstly, there are tracer differences between our study and those published, which will naturally be a source of variation. ^{11}C-PiB is a first generation amyloid-PET tracer, used widely by amyloid-PET studies. ^{18}F-Flutemetamol is a derivative of this, as a second generation tracer, with the ability to selectively bind to amyloid plaques similarly to ^{11}C-PiB (Vandenberghe et al., 2010). As described below, ^{18}F-Flutemetamol binds also to white matter, and as such there have historically been reports that this results in a higher number of amyloid positive classifications, e.g. in (Mountz et al., 2015). However, there have also been previous reports that ^{11}C-PiB binds to WM in older adults, as well as ^{18}F-Flutemetamol (Landau et al., 2014; Lowe et al., 2017). Nevertheless, a previous study from our laboratory has shown that there is a high concordance of ^{18}F-Flutemetamol and ^{11}C-PiB amyloid positivity classification when using the SUVR approach in the same individuals (94 % concordance rate in cognitively intact elderly participants) (Adamczuk et al., 2016), which has also been replicated by other centres in other (clinical) populations. In this previous study, there was a high correlation between ^{18}F-Flutemetamol and ^{11}C-PiB SUVR values, not only in the composite VOI ($\rho = 0.84$), but also in subcortical WM ($\rho = 0.82$). Previous studies comparing ^{18}F-labelled tracers, report that there are strong linear associations between the

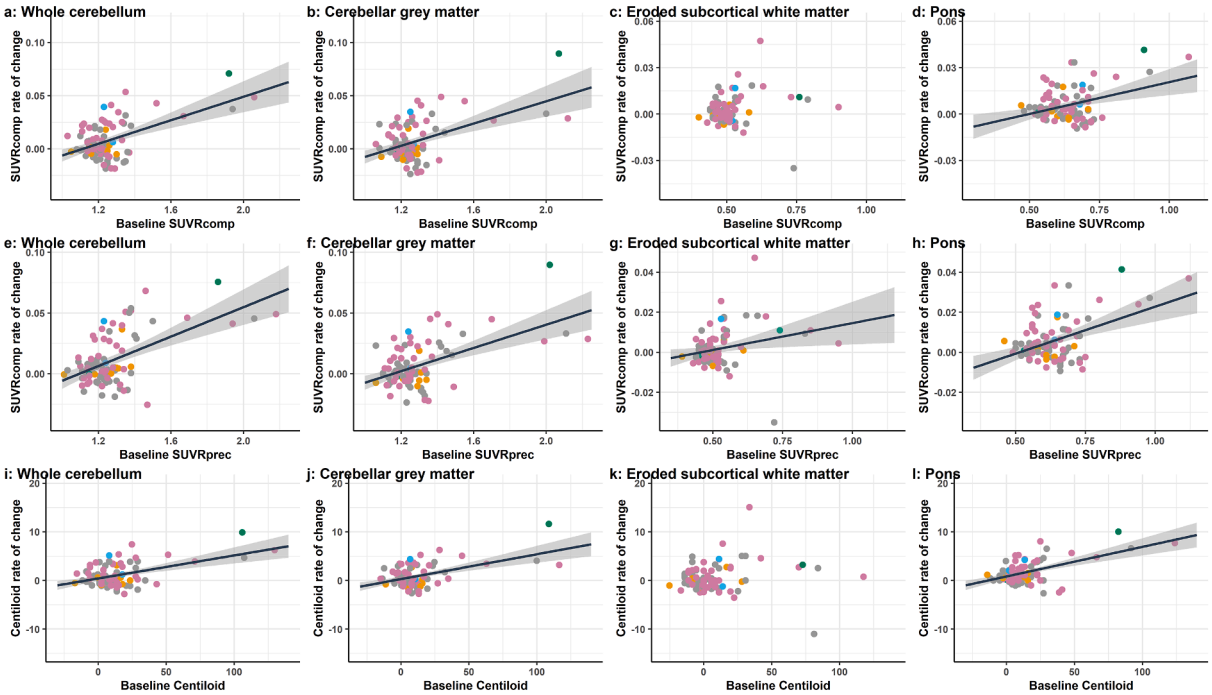

Fig. 4. Association between baseline amyloid load and composite cortical amyloid rate of change. Regressions for baseline $SUVR_{comp}$ and composite amyloid rate of change observed in (**a**) Whole cerebellum, (**b**) Cerebellar grey matter (**c**) Eroded subcortical white matter, (**d**) Pons. Association between baseline $SUVR_{prec}$ and composite amyloid rate of change observed in (**e**) Whole cerebellum, (**f**) Cerebellar grey matter, (**g**) Eroded subcortical white matter, (**h**) Pons. Association between baseline CL and composite amyloid rate of change in (**i**) Whole cerebellum, (**j**) Cerebellar grey matter (**k**) Eroded subcortical white matter, (**l**) Pons. Note the differing scales due to the nature of the values for the reference regions. Data points are coloured by *APOE4* genotype (orange $\varepsilon2\varepsilon3$ N = 7; green $\varepsilon2\varepsilon4$ N = 2; grey $\varepsilon3\varepsilon3$ N = 41; pink $\varepsilon3\varepsilon4$ N = 38; blue $\varepsilon4\varepsilon4$ = 2). N = 90. Abbreviations: $SUVR_{comp}$ = Standardised uptake value ratio in the composite region; $SUVR_{prec}$ = Standardised uptake value ratio in the precuneus. (For interpretation of the references to colour in this figure legend, the reader is referred to the web version of this article.)

different tracers, even in unmatched populations (Landau et al., 2014), and that there is a high agreement in amyloid positivity status, for example between ^{18}F-Flutemetamol and ^{18}F-Florbetaben (98.1 % concordance rate) (Cho et al., 2020), or to discriminate between AD cases and controls (Wong et al., 2010; Yeo et al., 2015).

Secondly, there is a known high tracer retention in WM, independent of amyloid deposition and clinical diagnosis. This is largely due to ^{18}F-labelled radiotracers being highly lipophilic and binding to myelin basic protein, despite the exact nature of the aspecific binding being poorly understood (Carotenuto et al., 2020). There are often age-related WM changes (Lowe et al., 2018), such as increasing white matter lesions (Murray et al., 2012), potentially making WM reference regions variable over time. These lesions are more likely to appear in the subcortical WM than the cerebellum (Bullich et al., 2017), and are thus susceptible to amyloid radiotracer binding. This may result in an underestimation of amyloid levels in cortical regions of interest and is different for the ^{18}F-amyloid tracers currently used. This further strengthens our results that a cerebellar reference region is better suited at detecting subtle *APOE4*-related brain amyloid changes, since this is less susceptible to off-target WM binding.

Thirdly, the WM reference region used here differs to that used in many published articles as there is no consensus on which and how the WM region should be defined when creating a WM reference VOI. For example, a study using ^{11}C-PiB PET used a WM reference region consisting of the subject-specific eroded WM segmentation, with the cerebellar and brainstem WM manually removed prior to analysis (Heeman et al., 2020). In another example, the WM reference region was created by defining a Freesurfer subcortical WM image and smoothing this 8 mm^3 to the ^{18}F-Florbetapir PET image, with a threshold of 0.7 to erode the WM voxels (Landau et al., 2015). As a final example, the WM reference VOI was created by taking the WM MRI segmentation and manually defining a mask around the centrum semiovale (Bullich et al., 2017). Furthermore, many published studies lack details on how they define the WM VOI, thus reducing the ability to create the exact reference region in further studies. As can be appreciated from these examples, methods of defining WM reference VOIs are variable and differ between centres, which in itself is a disadvantage in terms of replicability.

Lastly, a unique aspect of our study, and its greatest strength, is the notably long follow-up time period. Published studies that promote WM reference regions for longitudinal amyloid-PET studies largely have a follow-up time period of two years (Blautzik et al., 2017; Bullich et al., 2017; Chen et al., 2015; Landau et al., 2015). However, the shortest follow-up time interval in our study is already longer than this (3.4 years), where our median time interval is 6.2 years (highest interval 10.9 years). PET images often have a low signal-to-noise ratio, which may have a larger effect when the follow-up duration is shorter than longer ones. This is potentially due to the changes in amyloid over a short period being smaller than if this interval was longer relative to the noise present. Our time interval duration is large and so the signal-to-noise ratio may have less of an effect. As described above, there is a high tracer retention in WM and there are WM changes associated with age. Therefore, this may influence the superiority of WM as a reference region choice for longitudinal amyloid-PET studies, which has also been postulated before using ^{11}C-PiB (Lowe et al., 2018). We cannot exclude that with a shorter time interval results may have been different, however, this is something we cannot directly test with our data.

Many studies have found that amyloid accumulates during early AD stages in the precuneus, and that *APOE4* may alter this trajectory (Buckner et al., 2005; Insel et al., 2020; Mattsson et al., 2019; Mishra et al., 2018; Palmqvist et al., 2017; Villain et al., 2012; Villemagne et al., 2011). From our data we can ascertain that there are high levels of amyloid observed in this region (Fig. 2e-h), but amyloid rate of change was not significantly different between *APOE4* status with any of the

reference regions. Numerically, *APOE4* carriers had a higher amyloid rate of change, which suggests that although the precuneus can detect differences in amyloid rate of change, the composite region is more sensitive at detecting these amyloid changes in asymptomatic AD, given significance is observed with the composite VOI when WCER and CGM are used as reference regions, with high corresponding *t*-values.

The direct comparison of SUVRs is imperfect given the differing scales, therefore presenting as a limitation, as it is difficult to directly compare these values and results across reference regions. However, CLs were developed in order to standardise amyloid measurements between tracers or centres (Klunk et al., 2015), and are increasingly used. Hence, our CL analysis circumvents the need to directly compare SUVRs, given the conversion of these to the (comparable) CL scale. The SUVR results should be interpreted with caution if directly comparing results, however, the CL results confirm our major findings, thus they remain valid: both with and without the outlier, WCER as reference region shows a significantly higher amyloid rate of change in *APOE4* carriers compared to non-carriers, with a higher *t*-value than the analyses with the other reference regions.

Ideally, all CL measurements from all four reference regions should be identical for each participant. CL values are consistent visually between reference regions as observed in Fig. 2, however, when looking at Fig. 3, it can also be observed that CL values are lower when using ESWM. This was highlighted in our repeated measures analysis, in which there are significant differences between CL values across reference regions, with ESWM showing the most significant differences with the other reference regions. Altogether, the results suggest that choice of reference region does affect CL values, with the largest differences observed with ESWM and the other reference VOIs. This could be due to the off-target white matter binding as described above, resulting in an underestimation of amyloid load, and thus lower CL values.

Due to the limited number of individuals with certain *APOE* genotypes in this cohort (e.g. *ε4ε4*) we were unable to determine the dose-dependent effects of allele status on longitudinal amyloid accumulation. Although ^{18}F-labelled tracers perform in a similar manner discriminating AD cases from controls, methods of acquisition and semi-quantification differ between tracers, so results should be carefully considered when inferring effects with other tracers. Finally, due to the original study design and recruitment for F-PACK we only analysed the asymptomatic stage of AD, so results should also be carefully considered when examining further stages of AD.

5. Conclusion

The reliable measurement of amyloid accumulation in cognitively intact older adults is of importance. Longitudinal amyloid-PET has already been used as a potential surrogate marker for drug effects, and the asymptomatic phase of AD offers a potential window for more efficacious intervention. Reference region selection influences the ability to determine early differential effects of *APOE4*. We can confirm the presence of amyloid accumulation within individuals of F-PACK, where it is the whole cerebellum that most sensitively captures the effect of *APOE4* both with standardised uptake value ratios and Centiloids. This is the most optimal reference region that can be recommended for determining amyloid accumulation in an asymptomatic AD setting using ^{18}F-Flutemetamol.

CRediT authorship contribution statement

Emma S. Luckett: Data curation, Conceptualization, Investigation, Formal analysis, Visualization, Writing – original draft, Writing – review & editing. **Jolien Schaeverbeke: . Steffi De Meyer: . Katarzyna Adamczuk: . Koen Van Laere: . Patrick Dupont: . Rik Vandenbergh: .**

Declaration of Competing Interest

The authors declare that they have no known competing financial interests or personal relationships that could have appeared to influence the work reported in this paper.

Data availability

Data will be made available on request.

Acknowledgement

We would like to thank the staff of Nuclear Medicine, Neurology, and Radiology at the University Hospitals Leuven.

Funding

Funded by Stichting Alzheimer Onderzoek (#13007, 20170032), Vlaams Agentschap voor.

Innovatie en Onderzoek (ICON project HBC.2019.2523; Vlaams Initiatief voor Netwerken voor Dementie-onderzoek 3M140252), Flemish Research Foundation (JPND co-funding G0G1519N; G094418N).

The project leading to this application has received funding for the Innovative Medicines Initiative 2 Joint Undertaking under grant agreement No 115952 (http://www.imi.europa.eu). This Joint Undertaking receives the support from the European Union's Horizon 2020 research and innovation programme and EFPIA. This communication reflects the views of the authors and neither IMI nor the European Union and EFPIA are liable for any use that may be made of the information contained herein.

JS is a junior postdoctoral fellow of the Fonds Wetenschappelijk Onderzoek (FWO/Belgium, 12Y1620N) and Stichting Alzheimer association (#SAO-FRA 2021/00022).

SDM is a doctoral fellow of the Fonds voor Wetenschappelijk Onderzoek (FWO/Belgium, 11M0522N).

Conflicts of interest/competing interests

The tracer for the F-PACK baseline amyloid-PET scans was provided under a material transfer agreement between UZ Leuven and GE Healthcare free of charge. RV was the global PI of the phase 1 and 2 ^{18}F-Flutemetamol PET studies. RV's institution has clinical trial agreements (RV as PI) with AbbVie, Biogen, J&J, Novartis, NovoNordisk, Prevail, Roche, UCB and Wave. RV's institution has received consultancy fee (RV as consultant) from Roche and Cytox. RV's institution has contractual agreement (RV as participant) with AC Immune and Novartis for participation in Data Safety Monitoring Board.

KVL has clinical trial agreements for UZ/KU Leuven for Janssen Pharmaceuticals, Merck, GE Healthcare, Lundbeck, UCB, Cerveau, Syndesi, CHDI, Eikonizo, Curasen, BMS, and is a consultant for Cerveau and Sanofi.

KA is an employee of BioClinica.

Appendix A. Supplementary data

Supplementary data to this article can be found online at https://doi.org/10.1016/j.nicl.2023.103321.

References

Adamczuk, K., de Weer, A.S., Nelissen, N., Chen, K., Sleegers, K., Bettens, K., van Broeckhoven, C., Vandenbulcke, M., Thiyyagura, P., Dupont, P., van Laere, K., Reiman, E.M., Vandenberghe, R., 2013. Polymorphism of brain derived neurotrophic factor influences β amyloid load in cognitively intact apolipoprotein ε4 carriers. Neuroimage Clin. 2, 512–520. https://doi.org/10.1016/j.nicl.2013.04.001.

Adamczuk, K., Schaeverbeke, J., Nelissen, N., Neyens, V., Vandenbulcke, M., Goffin, K., Lilja, J., Hilven, K., Dupont, P., van Laere, K., Vandenberghe, R., 2016. Amyloid imaging in cognitively normal older adults: comparison between 18F-flutemetamol and 11C-Pittsburgh compound B. Eur. J. Nucl. Med. Mol. Imaging 43, 142–151. https://doi.org/10.1007/s00259-015-3156-9.

Blautzik, J., Brendel, M., Sauerbeck, J., Kotz, S., Scheiwein, F., Bartenstein, P., Seibyl, J., Rominger, A., 2017. Reference region selection and the association between the rate of amyloid accumulation over time and the baseline amyloid burden. Eur. J. Nucl. Med. Mol. Imaging 44 (8), 1364–1374. https://doi.org/10.1007/s00259-017-3666-8.

Buckner, R.L., Snyder, A.Z., Shannon, B.J., LaRossa, G., Sachs, R., Fotenos, A.F., Sheline, Y.I., Klunk, W.E., Mathis, C.A., Morris, J.C., Mintun, M.A., 2005. Molecular, structural, and functional characterization of Alzheimer's disease: Evidence for a relationship between default activity, amyloid, and memory. J. Neurosci. 25, 7709–7717. https://doi.org/10.1523/JNEUROSCI.2177-05.2005.

Bullich, S., Villemagne, V.L., Catafau, A.M., Jovalekic, A., Koglin, N., Rowe, C.C., de Santi, S., 2017. Optimal reference region to measure longitudinal amyloid-b change with 18F-Florbetaben PET. J. Nucl. Med. 58, 1300–1306. https://doi.org/10.2967/jnumed.116.187351.

Burnham, S.C., Laws, S.M., Budgeon, C.A., Doré, V., Porter, T., Bourgeat, P., Buckley, R. F., Murray, K., Ellis, K.A., Turlach, B.A., Salvado, O., Ames, D., Martins, R.N., Rentz, D., Masters, C.L., Rowe, C.C., Villemagne, V.L., 2020. Impact of APOE-ε4 carriage on the onset and rates of neocortical Aβ-amyloid deposition. Neurobiol. Aging 95, 46–55. https://doi.org/10.1016/j.neurobiolaging.2020.06.001.

Carotenuto, A., Giordano, B., Dervenoulas, G., Wilson, H., Veronese, M., Chappell, Z., Polychronis, S., Pagano, G., Mackewn, J., Turkheimer, F.E., Williams, S.C.R., Hammers, A., Silber, E., Brex, P., Politis, M., 2020. [18F]Florbetapir PET/MR imaging to assess demyelination in multiple sclerosis. Eur. J. Nucl. Med. Mol. Imaging 47, 366–378. https://doi.org/10.1007/s00259-019-04533-y.

Chen, K., Roontiva, A., Thiyyagura, P., Lee, W., Liu, X., Ayutyanont, N., Protas, H., Luo, J.L., Bauer, R., Reschke, C., Bandy, D., Koeppe, R.A., Fleisher, A.S., Caselli, R.J., Landau, S., Jagust, W.J., Weiner, M.W., Reiman, E.M., 2015. Improved power for characterizing longitudinal amyloid-βPET changes and evaluating amyloid-modifying treatments with a cerebral white matter reference region. J. Nucl. Med. 56, 560–566. https://doi.org/10.2967/jnumed.114.149732.

Chiao, P., Bedell, B.J., Avants, B., Zijdenbos, A.P., Grand'Maison, M., O'Neill, P., O'Gorman, J., Chen, T., Koeppe, R., 2019. Impact of reference and target region selection on amyloid PET SUV ratios in the phase 1B PRIME study of aducanumab. J. Nucl. Med. 60, 100–106. https://doi.org/10.2967/jnumed.118.209130.

Cho, S.H., Choe, Y.S., Kim, Y.J., Lee, B., Kim, H.J., Jang, H., Kim, J.P., Jung, Y.H., Kim, S. J., Kim, B.C., Farrar, G., Na, D.L., Moon, S.H., Seo, S.W., 2020. Concordance in detecting amyloid positivity between 18F-florbetaben and 18F-flutemetamol amyloid PET using quantitative and qualitative assessments. Sci. Rep. 10, 1–10. https://doi.org/10.1038/s41598-020-76102-5.

Corder, E.H., Saunders, A.M., Strittmatter, W.J., Schmechel, D.E., Gaskell, P.C., Small, G. W., Roses, A.D., Haines, J.L., Pericak-Vance, M.A., 1993. Gene dose of apolipoprotein E type 4 allele and the risk of Alzheimer's disease in late onset families. Science 1979 (261), 921–923. https://doi.org/10.1126/science.8346443.

de Meyer, S., Schaeverbeke, J.M., Verberk, I.M.W., Gille, B., de Schaepdryver, M., Luckett, E.S., Gabel, S., Bruffaerts, R., Mauroo, K., Thijssen, E.H., Stoops, E., Vanderstichele, H.M., Teunissen, C.E., Vandenberghe, R., Poesen, K., 2020. Comparison of ELISA- and SIMOA-based quantification of plasma Aβ ratios for early detection of cerebral amyloidosis. Alzheimers Res. Ther. 12, 162. https://doi.org/10.1186/s13195-020-00728-w.

Drzezga, A., Grimmer, T., Henriksen, G., Mühlau, M., Perneczky, R., Miederer, I., Praus, C., Sorg, C., Wohlschläger, A., Riemenschneider, M., Wester, H.J., Foerstl, H., Schwaiger, M., Kurz, A., 2009. Effect of APOE genotype on amyloid plaque load and gray matter volume in Alzheimer disease. Neurology 72, 1487–1494. https://doi.org/10.1212/WNL.0b013e3181a2e8d0.

Fleisher, A.S., Chen, K., Liu, X., Ayutyanont, N., Roontiva, A., Thiyyagura, P., Protas, H., Joshi, A.D., Sabbagh, M., Sadowsky, C.H., Sperling, R.A., Clark, C.M., Mintun, M.A., Pontecorvo, M.J., Coleman, R.E., Doraiswamy, P.M., Johnson, K.A., Carpenter, A.P., Skovronsky, D.M., Reiman, E.M., 2013. Apolipoprotein E ε4 and age effects on florbetapir positron emission tomography in healthy aging and Alzheimer disease. Neurobiol. Aging 34, 1–12. https://doi.org/10.1016/j.neurobiolaging.2012.04.017.

Grimmer, T., Tholen, S., Yousefi, B.H., Alexopoulos, P., Frschler, A., Frstl, H., Henriksen, G., Klunk, W.E., Mathis, C.A., Perneczky, R., Sorg, C., Kurz, A., Drzezga, A., 2010. Progression of cerebral amyloid load is associated with the apolipoprotein e ε4 genotype in Alzheimer's disease. Biol. Psychiatry 68, 879–884. https://doi.org/10.1016/j.biopsych.2010.05.013.

Heeman, F., Hendriks, J., Lopes Alves, I., Ossenkoppele, R., Tolboom, N., van Berckel, B. N.M., Lammertsma, A.A., Yaqub, M., 2020. [11C]PIB amyloid quantification: effect of reference region selection. EJNMMI Res. 10 (1) https://doi.org/10.1186/s13550-020-00714-1.

Hong, Y.J., Kim, C.M., Lee, J.H., Sepulcre, J., 2022. Correlations between APOE4 allele and regional amyloid and tau burdens in cognitively normal older individuals. Sci. Rep. 12, 14307. https://doi.org/10.1038/s41598-022-18325-2.

Insel, P.S., Mormino, E.C., Aisen, P.S., Thompson, W.K., Donohue, M.C., 2020. Neuroanatomical spread of amyloid β and tau in Alzheimer's disease: implications for primary prevention. Brain Commun. 2 https://doi.org/10.1093/braincomms/fcaa007.

Jack, C.R., Bennett, D.A., Blennow, K., Carrillo, M.C., Dunn, B., Haeberlein, S.B., Holtzman, D.M., Jagust, W., Jessen, F., Karlawish, J., Liu, E., Molinuevo, J.L., Montine, T., Phelps, C., Rankin, K.P., Rowe, C.C., Scheltens, P., Siemers, E., Snyder, H.M., Sperling, R., Elliott, C., Masliah, E., Ryan, L., Silverberg, N., 2018. NIA-AA Research Framework: Toward a biological definition of Alzheimer's disease. Alzheimer's Dementia 14 (4), 535–562. https://doi.org/10.1016/j.jalz.2018.02.018.

Klunk, W.E., Koeppe, R.A., Price, J.C., Benzinger, T.L., Devous, M.D., Jagust, W.J., Johnson, K.A., Mathis, C.A., Minhas, D., Pontecorvo, M.J., Rowe, C.C., Skovronsky, D.M., Mintun, M.A., 2015. The Centiloid project: Standardizing quantitative amyloid plaque estimation by PET. Alzheimer's Dementia 11, 1–15.e4. https://doi.org/10.1016/j.jalz.2014.07.003.

Koole, M., Lewis, D.M., Buckley, C., Nelissen, N., Vandenbulcke, M., Brooks, D.J., Vandenberghe, R., van Laere, K., 2009. Whole-body biodistribution and radiation dosimetry of 18F-GE067: A radioligand for in vivo brain amyloid imaging. J. Nucl. Med. 50, 818–822. https://doi.org/10.2967/jnumed.108.060756.

La Joie, R., Ayakta, N., Seeley, W.W., Borys, E., Boxer, A.L., DeCarli, C., Doré, V., Grinberg, L.T., Huang, E., Hwang, J.-H., Ikonomovic, M.D., Jack, C., Jagust, W.J., Jin, L.-W., Klunk, W.E., Kofler, J., Lesman-Segev, O.H., Lockhart, S.N., Lowe, V.J., Masters, C.L., Mathis, C.A., McLean, C.L., Miller, B.L., Mungas, D., O'Neil, J.P., Olichney, J.M., Parisi, J.E., Petersen, R.C., Rosen, H.J., Rowe, C.C., Spina, S., Vemuri, P., Villemagne, V.L., Murray, M.E., Rabinovici, G.D., 2019. Multisite study of the relationships between antemortem [11 C]PIB-PET Centiloid values and postmortem measures of Alzheimer's disease neuropathology. Alzheimer's Dementia 15 (2), 205–216. https://doi.org/10.1016/j.jalz.2018.09.001.

Landau, S.M., Thomas, B.A., Thurfjell, L., Schmidt, M., Margolin, R., Mintun, M., Pontecorvo, M., Baker, S.L., Jagust, W.J., 2014. Amyloid PET imaging in Alzheimer's disease: A comparison of three radiotracers. Eur. J. Nucl. Med. Mol. Imaging 41 (7), 1398–1407. https://doi.org/10.1007/s00259-014-2753-3.

Landau, S.M., Fero, A., Baker, S.L., Koeppe, R., Mintun, M., Chen, K., Reiman, E.M., Jagust, W.J., 2015. Measurement of longitudinal β-amyloid change with 18F-florbetapir PET and standardized uptake value ratios. J. Nucl. Med. 56, 567–574. https://doi.org/10.2967/jnumed.114.148981.

Lehmann, M., Ghosh, P.M., Madison, C., Karydas, A., Coppola, G., O'Neil, J.P., Huang, Y., Miller, B.L., Jagust, W.J., Rabinovici, G.D., 2014. Greater medial temporal hypometabolism and lower cortical amyloid burden in ApoE4-positive AD patients. J. Neurol. Neurosurg. Psychiatry 85, 266–273. https://doi.org/10.1136/jnnp-2013-305858.

Lim, Y.Y., Mormino, E.C., 2017. APOE genotype and early β-amyloid accumulation in older adults without dementia. Neurology 89 (10), 1028–1034. https://doi.org/10.1212/WNL.0000000000004336.

Lowe, V.J., Lundt, E., Knopman, D., Senjem, M.L., Gunter, J.L., Schwarz, C.G., Kemp, B. J., Jack, C.R., Petersen, R.C., 2017. Comparison of [18F]Flutemetamol and [11C] Pittsburgh Compound-B in cognitively normal young, cognitively normal elderly, and Alzheimer's disease dementia individuals. Neuroimage Clin. 16, 295–302. https://doi.org/10.1016/j.nicl.2017.08.011.

Lowe, V.J., Lundt, E.S., Senjem, M.L., Schwarz, C.G., Min, H.-K., Przybelski, S.A., Kantarci, K., Knopman, D., Petersen, R.C., Jack, C.R., 2018. White matter reference region in PET studies of 11C-Pittsburgh compound B uptake: Effects of age and amyloid-β deposition. J. Nucl. Med. 59 (10), 1583–1589. https://doi.org/10.2967/jnumed.117.204271.

Mattsson, N., Palmqvist, S., Stomrud, E., Vogel, J., Hansson, O., 2019. Staging β -Amyloid Pathology with Amyloid Positron Emission Tomography. JAMA Neurol. 76, 1319–1329. https://doi.org/10.1001/jamaneurol.2019.2214.

Minhas, D.S., Price, J.C., Laymon, C.M., Becker, C.R., Klunk, W.E., Tudorascu, D.L., Abrahamson, E.E., Hamilton, R.L., Kofler, J.K., Mathis, C.A., Lopez, O.L., Ikonomovic, M.D., 2018. Impact of partial volume correction on the regional correspondence between in vivo [C-11]PiB PET and postmortem measures of Aβ load. Neuroimage Clin. 19, 182–189. https://doi.org/10.1016/J.NICL.2018.04.007.

Mishra, S., Blazey, T.M., Holtzman, D.M., Cruchaga, C., Su, Y., Morris, J.C., Benzinger, T. L.S., Gordon, B.A., 2018. Longitudinal brain imaging in preclinical Alzheimer disease: Impact of APOE ϵ4 genotype. Brain 141, 1828–1839. https://doi.org/10.1093/brain/awy103.

Morris, J.C., Roe, C.M., Xiong, C., Fagan, A.M., Goate, A.M., Holtzman, D.M., Mintun, M. A., 2010. APOE predicts amyloid-beta but not tau Alzheimer pathology in cognitively normal aging. Ann. Neurol. 67, 122–131. https://doi.org/10.1002/ana.21843.

Mountz, J.M., Laymon, C.M., Cohen, A.D., Zhang, Z., Price, J.C., Boudhar, S., McDade, E., Aizenstein, H.J., Klunk, W.E., Mathis, C.A., 2015. Comparison of qualitative and quantitative imaging characteristics of [11C]PiB and [18F] flutemetamol in normal control and Alzheimer's subjects. Neuroimage Clin. 9, 592. https://doi.org/10.1016/J.NICL.2015.10.007.

Murray, M.E., Vemuri, P., Preboske, G.M., Murphy, M.C., Schweitzer, K.J., Parisi, J.E., Jack, C.R., Dickson, D.W., 2012. A quantitative postmortem MRI design sensitive to white matter hyperintensity differences and their relationship with underlying pathology. J. Neuropathol. Exp. Neurol. 71 (12), 1113–1122. https://doi.org/10.1097/NEN.0b013e318277387e.

Palmqvist, S., Schöll, M., Strandberg, O., Mattsson, N., Stomrud, E., Zetterberg, H., Blennow, K., Landau, S., Jagust, W., Hansson, O., 2017. Earliest accumulation of β-amyloid occurs within the default-mode network and concurrently affects brain connectivity. Nat. Commun. 8, 1–13. https://doi.org/10.1038/s41467-017-01150-x.

Reiman, E.M., Chen, K., Liu, X., Bandy, D., Yu, M., Lee, W., Ayutyanont, N., Keppler, J., Reeder, S.A., Langbaum, J.B.S., Alexander, G.E., Klunk, W.E., Mathis, C.A., Price, J. C., Aizensteini, H.J., DeKosky, S.T., Caselli, R.J., 2009. Fibrillar amyloid-β burden in cognitively normal people at 3 levels of genetic risk for Alzheimer's disease. PNAS 106, 6820–6825. https://doi.org/10.1073/pnas.0900345106.

Reinartz, M., Luckett, E.S., Schaeverbeke, J., De Meyer, S., Adamczuk, K., Thal, D.R., Van Laere, K., Dupont, P., Vandenberghe, R., 2022. Classification of 18F-Flutemetamol scans in cognitively normal older adults using machine learning trained with neuropathology as ground truth. Eur. J. Nucl. Med. Mol. Imaging 49 (11), 3772–3786. https://doi.org/10.1007/s00259-022-05808-7.

Rowe, C.C., Ellis, K.A., Rimajova, M., Bourgeat, P., Pike, K.E., Jones, G., Fripp, J., Tochon-Danguy, H., Morandeau, L., O'Keefe, G., Price, R., Raniga, P., Robins, P., Acosta, O., Lenzo, N., Szoeke, C., Salvado, O., Head, R., Martins, R., Masters, C.L., Ames, D., Villemagne, V.L., 2010. Amyloid imaging results from the Australian Imaging, Biomarkers and Lifestyle (AIBL) study of aging. Neurobiol. Aging 31, 1275–1283. https://doi.org/10.1016/j.neurobiolaging.2010.04.007.

Salloway, S., Gamez, J.E., Singh, U., Sadowsky, C.H., Villena, T., Sabbagh, M.N., Beach, T.G., Duara, R., Fleisher, A.S., Frey, K.A., Walker, Z., Hunjan, A., Escovar, Y. M., Agronin, M.E., Ross, J., Bozoki, A., Akinola, M., Shi, J., Vandenberghe, R., Ikonomovic, M.D., Sherwin, P.F., Farrar, G., Smith, A.P.L., Buckley, C.J., Thal, D.R., Zanette, M., Curtis, C., 2017. Performance of [18F]flutemetamol amyloid imaging against the neuritic plaque component of CERAD and the current (2012) NIA-AA recommendations for the neuropathologic diagnosis of Alzheimer's disease. Alzheimer's Dementia 9, 25–34. https://doi.org/10.1016/j.dadm.2017.06.001.

Schaeverbeke, J.M., Gabel, S., Meersmans, K., Luckett, E.S., De Meyer, S., Adamczuk, K., Nelissen, N., Goovaerts, V., Radwan, A., Sunaert, S., Dupont, P., Van Laere, K., Vandenberghe, R., 2021. Baseline cognition is the best predictor of 4-year cognitive change in cognitively intact older adults. Alzheimers Res. Ther. 13 https://doi.org/10.1186/s13195-021-00798-4.

Schaeverbeke, J., Luckett, E.S., Gabel, S., Reinartz, M., de Meyer, S., Cleynen, I., Sleegers, K., van Broeckhoven, C., Bormans, G., Serdons, K., van Laere, K., Dupont, P., Vandenberghe, R., 2022. Lack of association between bridging integrator 1 (BIN1) rs744373 polymorphism and tau-PET load in cognitively intact older adults. Alzheimer's Dementia: Transl. Res. Clin. Intervent. 8, e12227.

Schwarz, C.G., Gunter, J.L., Lowe, V.J., Weigand, S., Vemuri, P., Senjem, M.L., Petersen, R.C., Knopman, D.S., Jack, C.R., 2019. A Comparison of Partial Volume Correction Techniques for Measuring Change in Serial Amyloid PET SUVR. J. Alzheimer's Dis. 67, 181–195. https://doi.org/10.3233/JAD-180749.

Toledo, J.B., Habes, M., Sotiras, A., Bjerke, M., Fan, Y., Weiner, M.W., Shaw, L.M., Davatzikos, C., Trojanowski, J.Q., 2019. APOE Effect on Amyloid-β PET Spatial Distribution, Deposition Rate, and Cut-Points. J. Alzheimer's Dis. 69 (3), 783–793. https://doi.org/10.3233/JAD-181282.

Tzourio-Mazoyer, N., Landeau, B., Papathanassiou, D., Crivello, F., Etard, O., Delcroix, N., Mazoyer, B., Joliot, M., 2002. Automated anatomical labeling of activations in SPM using a macroscopic anatomical parcellation of the MNI MRI single-subject brain. Neuroimage 15, 273–289. https://doi.org/10.1006/nimg.2001.0978.

Vandenberghe, R., van Laere, K., Ivanoiu, A., Salmon, E., Bastin, C., Triau, E., Hasselbalch, S., Law, I., Andersen, A., Korner, A., Minthon, L., Garraux, G., Nelissen, N., Bormans, G., Buckley, C., Owenius, R., Thurfjell, L., Farrar, G., Brooks, D.J., 2010. 18F-flutemetamol amyloid imaging in Alzheimer disease and mild cognitive impairment a phase 2 trial. Ann. Neurol. 68, 319–329. https://doi.org/10.1002/ana.22068.

Villain, N., Chételat, G., Grassiot, B., Bourgeat, P., Jones, G., Ellis, K.A., Ames, D., Martins, R.N., Eustache, F., Salvado, O., Masters, C.L., Rowe, C.C., Villemagne, V.L., 2012. Regional dynamics of amyloid-β deposition in healthy elderly, mild cognitive impairment and Alzheimer's disease: A voxelwise PiB-PET longitudinal study. Brain 135, 2126–2139. https://doi.org/10.1093/brain/aws125.

Villemagne, V.L., Pike, K.E., Chételat, G., Ellis, K.A., Mulligan, R.S., Bourgeat, P., Ackermann, U., Jones, G., Szoeke, C., Salvado, O., Martins, R., O'Keefe, G., Mathis, C.A., Klunk, W.E., Ames, D., Masters, C.L., Rowe, C.C., 2011. Longitudinal assessment of Aβ and cognition in aging and Alzheimer disease. Ann. Neurol. 69, 181–192. https://doi.org/10.1002/ana.22248.

Villemagne, V.L., Burnham, S., Bourgeat, P., Brown, B., Ellis, K.A., Salvado, O., Szoeke, C., Macaulay, S.L., Martins, R., Maruff, P., Ames, D., Rowe, C.C., Masters, C. L., 2013. Amyloid β deposition, neurodegeneration, and cognitive decline in sporadic Alzheimer's disease: A prospective cohort study. Lancet Neurol. 12, 357–367. https://doi.org/10.1016/S1474-4422(13)70044-9.

Vlassenko, A.G., Benzinger, T.L.S., Morris, J.C., 2012. PET amyloid-beta imaging in preclinical Alzheimer's disease. Biochim. Biophys. Acta Mol. Basis Dis. 1822 (3), 370–379. https://doi.org/10.1016/j.bbadis.2011.11.005.

Wong, D.F., Rosenberg, P.B., Zhou, Y., Kumar, A., Raymont, V., Ravert, H.T., Dannals, R. F., Nandi, A., Brašić, J.R., Ye, W., Hilton, J., Lyketsos, C., Kung, H.F., Joshi, A.D., Skovronsky, D.M., Pontecorvo, M.J., 2010. In Vivo Imaging of Amyloid Deposition in Alzheimer's Disease using the Novel Radioligand [18F]AV-45 (Florbetapir F 18). J. Nucl. Med. 51, 913. https://doi.org/10.2967/JNUMED.109.069088.

Yamazaki, Y.u., Zhao, N.a., Caulfield, T.R., Liu, C.-C., Bu, G., 2019. Apolipoprotein E and Alzheimer disease: pathobiology and targeting strategies. Nat. Rev. Neurol. 15 (9), 501–518. https://doi.org/10.1038/s41582-019-0228-7.

Yeo, J.M., Waddell, B., Khan, Z., Pal, S., 2015. A systematic review and meta-analysis of 18F-labeled amyloid imaging in Alzheimer's disease. Alzheimer's Dementia: Diagn., Assess. Dis. Monit. 1, 5–13. https://doi.org/10.1016/J.DADM.2014.11.004.